JOURNAL OF MATERIALS SCIENCE **36** (2001) 3769–3775

The brittle to ductile transition of single crystal materials—An indentation model

H. Y. LIN
Department of Materials Science and Engineering, National Tsing Hua University, Hsinchu, Taiwan

J. L. CHU, T. C. WU
Mechanical Industry Research Laboratories, Industrial Technology Research Institute, Chutung, Hsinchu, Taiwan

SANBOH LEE
Department of Materials Science and Engineering, National Tsing Hua University, Hsinchu, Taiwan

A model for the brittle to ductile transition of brittle single crystal materials under indentation has been investigated. Continuous dislocation pile-ups against the wedge tip are used to explain the plastic deformation. The indentation depth is attributed to the dislocation pile-ups. The critical indentation depth p_c of brittle to ductile transition is proposed. Thus, the single crystal material is in brittle mode during the indentation loading if the indentation depth is greater than p_c. Otherwise, it is ductile. Micrographs support this modeling. Indentation on the surfaces of (100) or (110) in fcc and bcc single crystal materials is compared. The parameter S is proportional to the number of dislocations and to the reciprocal of wedge angle. The value of S is smaller for (100) than for (110) in fcc structure, but the trend of bcc structure is opposite. The shape of indenter is similar to that of grinding particles consisting in cutting tools. In order to maintain cutting efficiency in ductile mode, the cutting tool must be replaced if the grinding particles are blunt.
© *2001 Kluwer Academic Publishers*

1. Introduction

Single crystal silicon is widely used in semiconductor manufacture, specifically, for the production of integrated circuits, large integrated circuits, and very large integrated circuits, etc.. The machining process of silicon wafers is the critical step to achieve the high quality of semiconductor devices. Stresses near the surface and subsurface are unavoidable during the machining. Mechanical damage appears if these stresses are large enough to generate dislocations or cracks [1, 2]. These dislocations or cracks alter the diffusion of impurities, electron-hole recombination, etc.. Thus, understanding the machining process of single crystal silicon is a key issue in semiconductor manufacturing.

The brittle versus ductile behavior of a material with crack has been extensively studied. According to Dieter [3], fracture requires only little energy for a brittle material, and a significant amount of energy for a ductile material. Khantha *et al.* [4] and Khantha [5] observed that the transition from brittle cleavage to ductile failure is attributed to a massive generation of dislocations arising from a cooperative Kosterlitz–Thouless type instability in single crystal silicon. Roberts *et al.* [6] used a computer simulation of the dislocation dynamics near a crack tip to explain the experimental data of a brittle to ductile transition. Roberts *et al.* [7] found the activation energy for the brittle to ductile transition is equal to that of dislocation glide in silicon, germanium and sapphire. Hirsch and Roberts [8] analyzed the strain-rate dependence of the sharp transition temperature. Rice and Thomson [9] proposed a spontaneous dislocation emission criterion and analyzed the brittle to ductile transition for different materials. Zhang [10], Chang and Ohr [11], Lee and coworkers [12–14] also studied the ductile versus brittle transition based on continuum dislocation theory and discrete dislocation pile-ups. Those researchers concentrated on the brittle versus ductile behavior of material with a crack appearing before the mechanical loading and concerned the intrinsic properties of materials. They did not consider a crack-free material prior to loading.

In this paragraph, the material is considered intrinsically brittle. Before cutting, the single crystal material is assumed to be crack-free. For example, Fig. 1 shows the morphology of a machined (111) plane in single crystal silicon. The cutting depth increases from the upper-right to lower-left direction. It can be seen from the figure that the upper-right region (look like the fine parallel stripes) is ductile and the lower-left region (look like the coarse irregular stripe) is brittle. The brittle to ductile transition region is located at the diagonal line where the depth is between 0.5 and 0.8 μm.

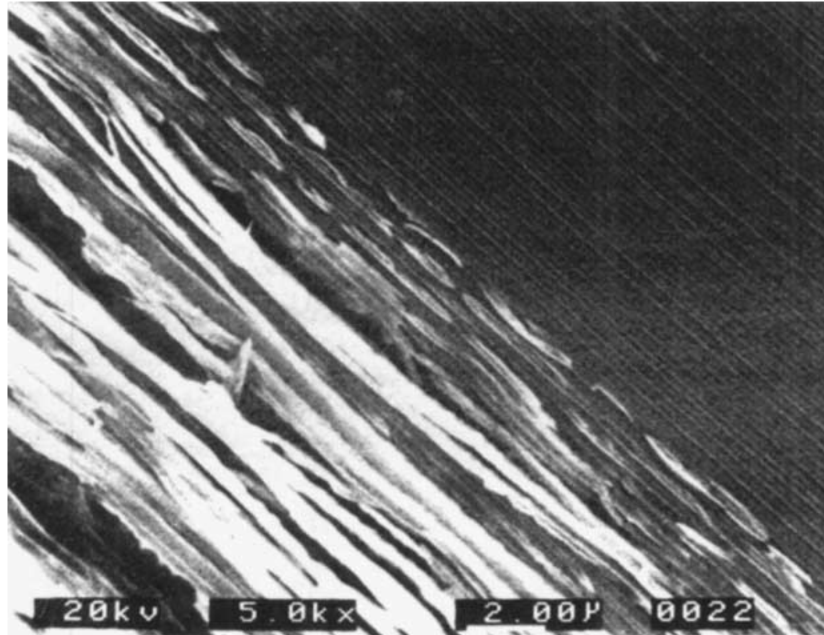

Figure 1 A SEM micrograph of machined silicon (111) plane by a ruling tool where the turning speed is 3000 rpm and cross feed speed is 80 nm/revolution.

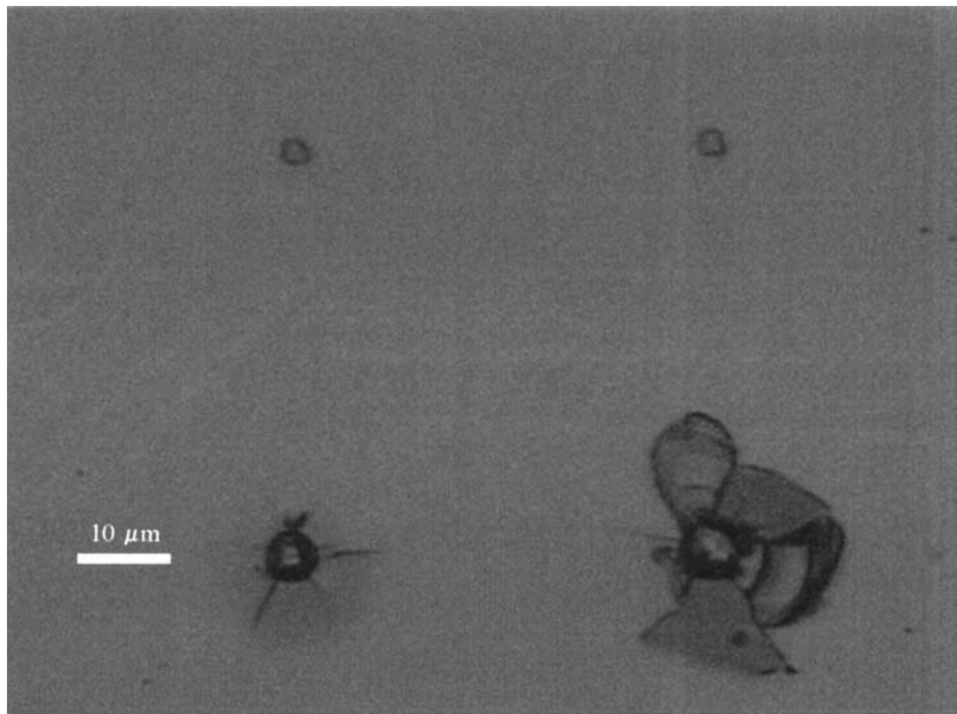

Figure 2 A micrograph of silicon (100) plane under a spherical indenter of tip radius 5 μm. The upper and lower morphologies are subject to 200 and 400 mN, respectively.

The brittle to ductile transition of material removal under cutting was also studied by Nakasuji *et al*. [15]. Cleavage behaves in a brittle manner whereas plastic deformation behaves in a ductile manner. The brittle to ductile transition of material removal was analyzed based on molecular dynamics simulation [16, 17]. For simplification, both indentation and scratch tests are often used to simulate the machining problem. However, indentation-induced phase transformations have been observed [18, 19]. Recently, we observed the brittle to ductile transition of silicon at a load between 200 mN and 400 mN using a spherical nano-indenter of tip radius 5 μm (see Fig. 2). It prompted us to study the brittle to ductile transition of a single crystal material using a wedge indenter. We propose a simple model based on the dislocation nucleation and motion under the indentation to explain the brittle versus ductile behavior. Furthermore, based on this criterion, we analyze the indenter acting on the (100) or (110) planes in fcc and bcc single crystal materials.

2. Brittle to ductile transition analysis

2.1. Dislocation pile-ups

The problem is shown in Fig. 3. A wedge indenter is normal to the free surface (100) of single crystal

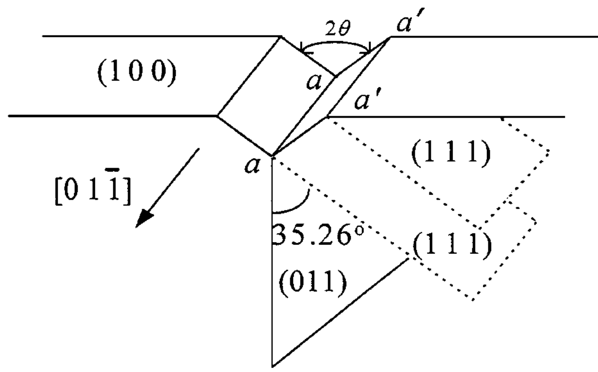

Figure 3 A schematic diagram of single crystal silicon under indentation loading.

silicon. The indentation line (intersection between the wedge indenter and silicon) is in the $[01\bar{1}]$ direction. The wedge angle of the indenter is 2θ. Assume that the free surface is flat before the load is applied. Under action of the load, the displacement and stress fields near the tip build up and the maximum shear stress is located at the wedge tip. Although the loading stress is less than the friction stress, the stress at the wedge tip (stress concentration) is possibly greater than the friction stress. During loading, dislocations emanate from the wedge tip and move away in its slip plane as soon as its shear stress becomes greater than the critical resolved shear stress. Note that the indentation-induced phase transformations are not considered because the energy consumed by the dislocation is much greater than that by indentation-induced phase transformation. Upon unloading, some incipient dislocations retreat back to the wedge tip and the rest of the dislocations pile up near the wedge tip. During loading, the indentation depth is due to both elastic deformation and plastic deformation [12, 14]. The elastic displacement recovers after load removal so that after loading the indentation depth is completely due to the plastic deformation. For crystalline materials, the plastic deformation is dominated by dislocation pile-ups.

Assume that the indentation depth is fully produced by dislocations. The dislocations of infinitesimal Burgers vector D(x)dx are parallel to each other and line up against the wedge tip from the positive x-axis upon unloading where D(x) is the dislocation density between x and x + dx. The piled-up length is L. The force equilibrium [20] is written as

$$\frac{G}{2\pi(1-\nu)}\int_0^L \frac{D(x)}{x'-x}\,dx = \sigma_f \quad \text{for } 0 < x < L \tag{1}$$

where G, ν and σ_f are the shear modulus, Poisson's ratio and the friction stress, respectively. The total Burgers vector nb is

$$\int_0^L D(x)\,dx = nb \tag{2}$$

The solution of Equation 1 with Equation 2 is [20]

$$D(x) = \frac{4nb}{\pi L}\sqrt{\frac{L-x}{x}} \quad \text{for } 0 \leqq x \leqq L \tag{3}$$

where

$$L = \frac{Gnb}{\pi\sigma_f(1-\nu)} \tag{4}$$

Although the above derivation is valid in an infinite medium, this is a good approximation for dislocation pile-ups against a free surface based on the numerical calculation. The error is less than 10% for edge dislocation. However, the analytical solution for a semi-infinite medium is not available. The purpose of this study is to explain qualitatively the brittle to ductile transition so that the above approximation is reasonably adopted. The detailed analysis will be in the future.

2.2. Indentation depth

The slip plane of single crystal silicon is $(\bar{1}\bar{1}1)$ and the vertical plane consisting of the wedge tip is $(\bar{1}\bar{1}0)$, i.e., the angle between these two planes is 35.26° as shown in Fig. 3. If the wedge angle is 70.53°, the dislocation slip occurs at positions a and a' as shown in Fig. 4a. As stated in the previous section, the indentation depth p along the direction [112] is attributed to the dislocation slip. Then the total Burgers vectors nb along ac and $a'c'$ is

$$nb = \sqrt{6}p/4 \tag{5}$$

If the wedge angle is slightly different from 70.53°, the other slip systems would occur as shown in Fig. 4b and c. However, the primary slip system is still dominated by those of the wedge angle 70.53°. Therefore, the total Burgers vector along ac and $a'c'$ is modified as

$$nb = p\sin\theta/\sin(\theta + 35.26°) \tag{6}$$

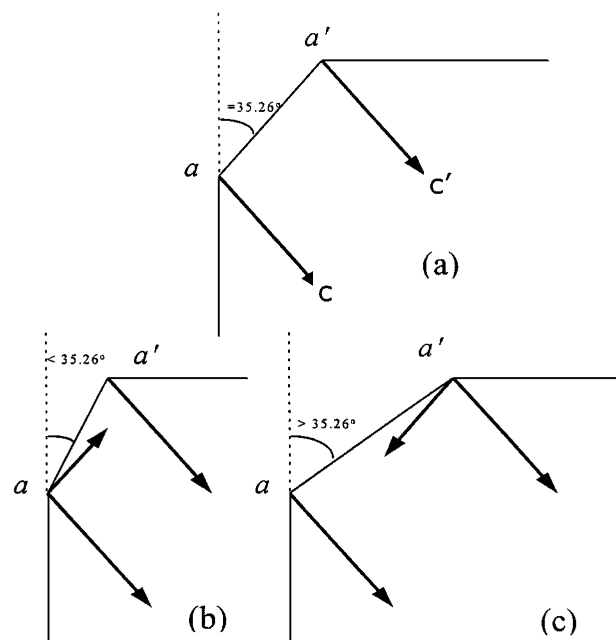

Figure 4 The slip systems for different wedge angles: (a) $\theta = 35.26°$; (b) $\theta < 35.26°$; (c) $\theta > 35.26°$.

where θ is half wedge angle defined before. n increases with increasing θ for θ smaller than 90°.

2.3. Brittle to ductile transition criterion

Under the action of indentation loading, the plastic deformation of single crystal silicon is due to dislocation movement. If the mobility of dislocations is low enough, the dislocations cannot move and a crack nucleus is formed. The mechanical failure of the single crystal silicon is attributed to fracture and the material is brittle. According to Stroh [21], a crack nucleus is formed when two leading dislocations in a pile-up are forced to separate within a distance of one Burgers vector. That is, the dislocation density near the wedge tip satisfies the equation,

$$\int_0^b D(x)\,dx > b \tag{7}$$

Substituting Equations 3, 4 and 6 into Equation 7, we obtain

$$p > p_c = \frac{\pi G b}{16\sigma_f(1-\nu)} \frac{\sin(\theta + 35.26°)}{\sin\theta} \tag{8}$$

where p_c is the critical indentation depth of brittle to ductile transition. If the indentation depth satisfies Equation 8, a brittle behavior is expected. Otherwise, the single crystal silicon is ductile under this process.

3. Micromachining modeling

The micromachining tool consists of many grinding particles. Under an action of compression load, grinding particles move and cut a thin layer of brittle material. The cutting process is simply simulated by the indentation and scratching. The indentation is analyzed in the present study while the scratching will be studied in the future. Each grinding particle may be considered as a wedge indenter. Although we concentrated on single crystal silicon in the previous section, this treatment can be extended to other brittle materials. Here and after, we consider a wedge indenter acting on a brittle single crystal material. The total Burgers vector nb along the slip direction is proportional to the indentation depth p and Equation 6 is modified as

$$nb = Sp \tag{9}$$

where S is a function of crystal structure, indentation plane, indentation angle, slip plane, etc.. According to Equation 9, for a given indentation depth, the value of S increases with number of dislocations in the single crystal material (or work piece). More dislocations imply more pronounced work hardening. After reach this indentation depth, it is harder to create dislocation. That is, the material becomes brittle.

Mechanical damage depends on the crystal orientation and structure. It is reasonable to extend the critical indentation depth p_c from single crystal silicon (see Equation 8) to brittle single crystal material,

$$p_c = \frac{\pi G b}{16\sigma_f(1-\nu)} \frac{1}{S} \tag{10}$$

For the same shear modulus, Poisson's ratio, and friction stress, the critical indentation depth is inversely proportional to the parameter, S. According to Equation 10, if the value of S increases, the critical indentation depth decreases. This implies that the cutting depth decreases with increasing S for machining brittle material in the ductile regime.

A comparison of experiments with the present model is made. First, Fig. 1 shows a SEM micrograph of a (111) plane in single crystal silicon machined by a ruling tool. The ruling tool with a cross feed speed of 80 nm/revolution moves along the diagonal line from the upper-right to the lower-left region so that the cutting depth is small in the upper-right region and large in the lower-left region. The upper-right region is ductile whereas the lower-left region is brittle. The diagonal line at the depth between 0.5 and 0.8 μm is a critical cutting depth of the brittle to ductile transition. Second, upper and lower indentation morphologies of single crystal silicon subjected to 200 mN and 400 mN are shown in Fig. 2. It can be seen from Fig. 2 that no crack appears in the region around the upper indentation and many cracks are observed in the region near the lower indentation. Because the indentation depth is proportional to the applied force, the upper indentation has a smaller indentation depth than the lower indentation. The critical indentation depth is located at a load between 200 mN and 400 mN. In summary, both experimental observations are good agreement with our prediction.

4. *S* function

4.1. Derivation of *S* Function

From the previous section, the parameter S plays a very important role on micromachining. According to Fig. 3, if lines aa and $a'a'$ are parallel to each other, the parameter S can be extended from the single crystal silicon (Equation 6) to a brittle single crystal material as

$$S = \sin\theta / \sin(\theta + \theta_s) \tag{11}$$

where θ_s is the angle between slip plane and vertical plane. Tables I and II list some values of θ_s in fcc and bcc structures, respectively. On the other hand, if two lines of aa and $a'a'$ are not parallel, i.e., the angle between these two lines is ϕ, then θ in Equation 11 should be replaced by $\theta_1 = \tan^{-1}(\tan\theta/\cos\phi)$ and the length becomes shortened by a factor of $\cos\phi$ (see Fig. 5). Therefore, Equation 11 becomes

$$S = \sin\theta_1 \cos\phi / \sin(\theta_1 + \theta_s) \tag{12}$$

Furthermore, if the several slip planes occur simultaneously under the indentation, then Equation 11 is

TABLE I Indentation plane, *aa* line and slip planes of fcc structure with the corresponding angles θ_s.

Indenatation plane	*aa* line	slip plane	θ_s
(100)	[011]	$(1\bar{1}1),(11\bar{1})$	$\pm\tan^{-1}(1/\sqrt{2}) \cong \pm 35.26°$
	$[01\bar{1}]$	$(111),(1\bar{1}\bar{1})$	$\pm\tan^{-1}(1/\sqrt{2}) \cong \pm 35.26°$
(110)	$[1\bar{1}0]$	$(111),(11\bar{1})$	$\pm\tan^{-1}\sqrt{2} \cong \pm 54.74°$
	$[1\bar{1}2]$	$(1\bar{1}\bar{1})$	0°
	$[1\bar{1}\bar{2}]$	$(1\bar{1}1)$	0°
(111)	$[1\bar{1}0]$	$(11\bar{1})$	$\pm\tan^{-1}(\sqrt{2}/4) \cong \pm 19.47°$
	$[10\bar{1}]$	$(1\bar{1}1)$	$\pm\tan^{-1}(\sqrt{2}/4) \cong \pm 19.47°$
	$[01\bar{1}]$	$(1\bar{1}\bar{1})$	$\pm\tan^{-1}(\sqrt{2}/4) \cong \pm 19.47°$

TABLE II Indentation plane, *aa* line and slip planes of bcc structure with the corresponding angles θ_s.

Indentation plane	*aa* line	slip plane	θ_s
(100)	[010]	$(10\bar{1}),(101)$	±45°
	[001]	$(101),(10\bar{1})$	±45°
	[011]	$(01\bar{1})$	0°
	$[01\bar{1}]$	(011)	0°
(110)	[001]	$(1\bar{1}0)$	0°
(110)	$[1\bar{1}\bar{1}]$	$(101),(01\bar{1})$	±30°
	$[1\bar{1}1]$	$(10\bar{1}),(011)$	±30°

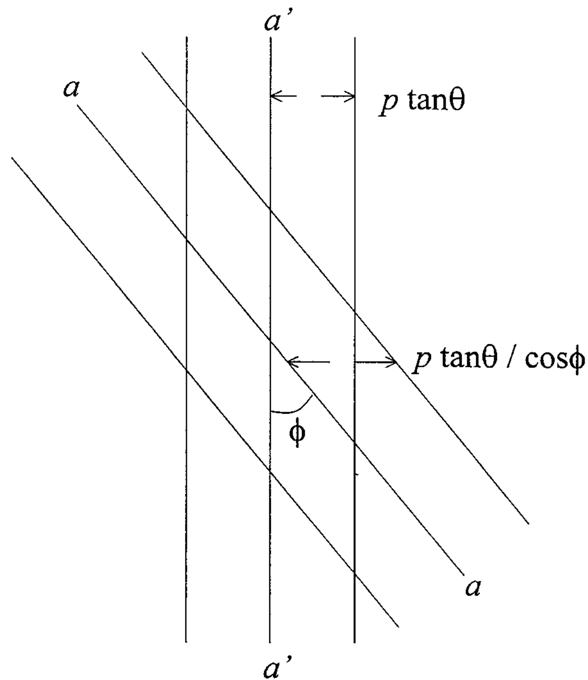

Figure 5 The schematic of lines *aa* and *a′a′*.

modified as

$$S = \sum_{i=1}^{m} \sin\theta_i \cos\phi_i / \sin(\theta_i + \theta_{s,i}). \qquad (13)$$

where $\theta_i = \tan^{-1}(\tan\theta/\cos\phi_i)$ and m is the number of slip planes. ϕ_i is the angle between both lines aa and $a'a'$ and $\theta_{s,i}$ is the angle between the ith slip plane and vertical plane.

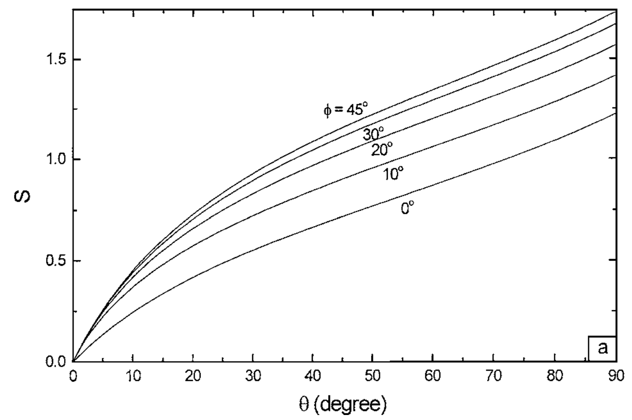

(a)

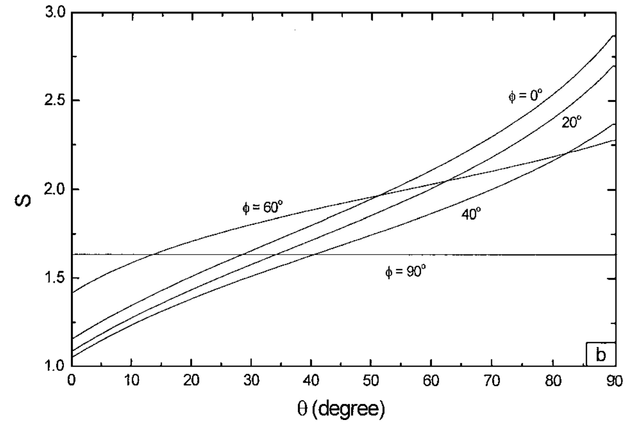

(b)

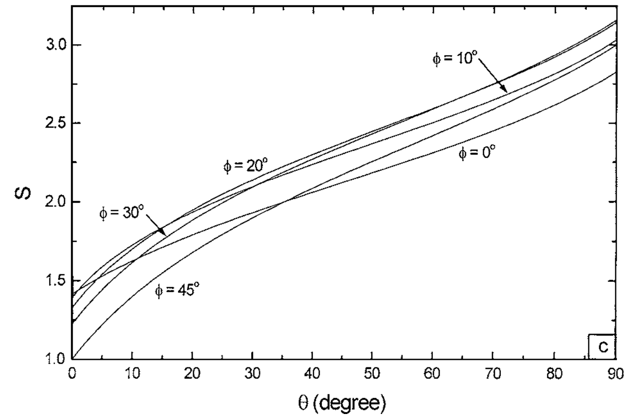

(c)

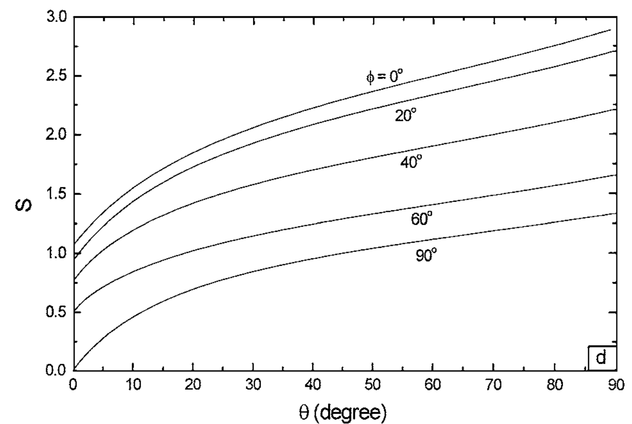

(d)

Figure 6 The curves of S versus the half wedge angle θ with various ϕ: (a) Indentation on (100) plane of fcc structure, (b) Indentation on (110) plane of fcc structure, (c) Indentation on (100) plane of bcc structure, and (d) Indentation on (110) plane of bcc structure.

4.2. Numerical results of S function

Assume that the dislocation slips in the {111} and {110} plane systems in the fcc and bcc single crystals, respectively, and a load is indented on the free surfaces (indentation plane) (100) and (110). From Tables I and II and Equation 13, we obtain the function S,

$$S_{fcc,100} = \frac{\sin\theta_1 \cos\phi}{\sin(\theta_1 + 35.26^\circ)} + \frac{\sin\theta_2 \cos(90^\circ - \phi)}{\sin(\theta_2 + 35.26^\circ)} \tag{14a}$$

$$S_{fcc,110} = \frac{\sin\theta_1 \cos\phi}{\sin(\theta_1 + 54.74^\circ)} + |\cos(54.74^\circ + \phi)| + \cos(54.74^\circ - \phi) \tag{14b}$$

$$S_{bcc,100} = \frac{\sin\theta_1 \cos\phi}{\sin(\theta_1 + 45^\circ)} + \frac{\sin\theta_2 \cos(90^\circ - \phi)}{\sin(\theta_2 + 45^\circ)} + |\cos(45^\circ + \phi)| + \cos(45^\circ - \phi) \tag{14c}$$

$$S_{bcc,110} = \cos\phi + \frac{\sin\theta_3 |\cos(35.26^\circ + \phi)|}{\sin(\theta_3 + 30^\circ)} + \frac{\sin\theta_4 \cos(35.26^\circ - \phi)}{\sin(\theta_4 + 30^\circ)} \tag{14d}$$

respectively, where

$$\theta_1 = \tan^{-1}(\tan\theta / \cos\phi) \tag{15a}$$

$$\theta_2 = \tan^{-1}[\tan\theta / \cos(90^\circ - \phi)] \tag{15b}$$

$$\theta_3 = \tan^{-1}[\tan\theta / |\cos(35.26^\circ + \phi)|] \tag{15c}$$

$$\theta_4 = \tan^{-1}[\tan\theta / \cos(35.26^\circ - \phi)] \tag{15d}$$

Fig. 6a shows the curves of $S_{\text{fcc},100}$ versus the half wedge angle θ with various values of ϕ. S increases with θ and ϕ. Instead of indentation plane (100), the values of S for indentation plane (110) are plotted in Fig. 6b. For a given θ, S oscillates with ϕ. The curves of $S_{\text{bcc},100}$ and $S_{\text{bcc},110}$ versus the half wedge angle θ with various values of ϕ are plotted in Fig. 6c and d, respectively. For a given θ, S oscillates with ϕ for indentation plane (100) and decreases monotonically with increasing ϕ for indentation plane (110).

For a given ϕ, S increases monotonically with increasing θ for both indentation plane and crystal structure with the exception of the line $\phi = 0$ where the indenter acts on the plane (110) in fcc structure. When the wedge angle increases, the critical indentation depth decreases. This implies that the cutting depth of brittle material within the ductile regime is reduced. In order to cut efficiently in the ductile mode, the cut blade must be replaced if its grinding particle is blunt. Comparing Figs 6a and b, the value of S is smaller for (100) plane than for (111) plane in fcc structure, but the trend for the bcc structure is opposite (see Fig. 6c and d).

5. Summary

An indenter is used to simulate the single grinding particle of the cutting tool. A model based on dislocation pile-ups is proposed to explain the brittle to ductile transition in brittle single crystal materials during indentation loading. The indentation depth is due to the dislocation motion. If the Burgers vector of a continuous dislocation within a distance of one Burgers vector from the wedge tip is larger than one Burgers vector, a crack nucleus is assumed to be generated. Based on this assumption, we define the critical indentation depth p_c that is increased linearly with the shear modulus and Burgers vector, and inversely proportional to the friction stress and parameter S. The parameter S depends on the crystal structure and orientation. If the indentation depth is greater than p_c, the material will be cut in a brittle regime. Otherwise, it is ductile. Experimental evidence is provided with both ruling tool and nano-indentation.

We compare a load indented on the (100) and (110) faces in the fcc and bcc structure. The value of S for the indentation plane (100) in the fcc structure is smaller than that for (110), but the trend for bcc structure is opposite. This implies that cutting is more brittle on (110) than on (100) at the same indentation depth for the fcc structure, but the trend of bcc structure is opposite. The value of S increases with increasing wedge angle regardless of crystal structure and indentation plane. This is equivalent to that the wedge angle increases with decreasing critical indentation depth. For keeping cutting in ductile mode, the indentation depth decreases with increasing wedge angle. Furthermore, in order to maintain the cutting efficiency in ductile mode, the cutting blade must be replaced if the grinding particle is blunt.

Acknowledgment

This work was partially supported by the National Science Council, Taiwan.

References

1. U. BISMAGER, E. BRINKSMERIER, B. GÜTTER, H. SEIBT and C. MENZ, *Precision Engineering* **16** (1994) 139.
2. E. BRINKSMERIER, *ibid.* **11** (1989) 211.
3. D. BROEK, "Elementary Engineering Fracture Mechanics," 4th ed. (Martinus Nijhoff Publishers, Boston, MA, 1986), Chaps 2, 11.
4. M. KHANTHA, D. P. POPE and V. VITEK, *Physical Review Letter* **73**(5) (1994) 684.
5. M. KHANTHA, *Scripta Metall. Mater.* **31**(10) (1994) 1355.
6. S. G. ROBERTS, M. ELLIS and P. B. HIRSCH, *Mater. Sci. Eng.* **A164** (1993) 135.
7. S. G. ROBERTS, A. S. BOOTH and P. B. HIRSCH, *ibid.* **A176** (1994) 91.
8. P. B. HIRSCH and S. G. ROBERTS, *Acta Metall. Mater.* **44**(6) (1996) 2361.
9. J. R. RICE and R. THOMSON, *Phil. Mag.* **29** (1974) 73.
10. T. Y. ZHANG, *Z. Metallkd.* **81** (1990) 63.
11. S. J. CHANG and S. M. OHR, *J. Appl. Phys.* **53** (1982) 5645.
12. S. T. SHIUE and S. LEE, *Phil. Mag.* **A61** (1990) 85.
13. S. LEE, *Key Eng. Mater.* **145–149** (1997) 135.
14. C. C. HUANG, C. C. YU and S. LEE, *J. Mater. Res.* **10** (1995) 183.
15. T. NAKASUJI, S. KODERA, S. HARA, H. MATSUNAGA, N. IKAWA and S. SHIMADA, *Annals of the CIRP* **39** (1990) 89.
16. S. SHIMADA, N. IKAWA, T. INAMURA, N. TAKEZAWA, H. OHMORI and T. SATA, *ibid.* **44** (1995) 523.
17. T. INAMURA, S. SHIMADA, N. TAKEZAWA and N. NAKAHARA, *ibid.* **46** (1997) 31.

18. D. R. CLARKE, M. C. KROLL, P. D. KIRCHNER, R. F. COOK and B. J. HOCKEY, *Phys. Rev. Lett.* **60** (1988) 2156.
19. G. M. PHARR, W. C. OLIVER and D. S. HARDING, *J. Mat. Res.* **6** (1991) 1129.
20. J. WEERTMAN and J. R. WEERTMAN, "Elementary Dislocation Theory," (Macmillan, New York, 1964) p. 129.
21. A. N. STROH, *Advanced Physics* **6** (1957) 418.

Received 7 February 2000
and accepted 6 February 2001